Results in Physics 39 (2022) 105797

Contents lists available at ScienceDirect

Results in Physics

journal homepage: www.elsevier.com/locate/rinp

The effect of the Caputo fractional difference operator on a new discrete COVID-19 model

Abderrahmane Abbes [a,*], Adel Ouannas [b], Nabil Shawagfeh [a], Giuseppe Grassi [c]

[a] Department of Mathematics, The University of Jordan, Amman, 11942, Jordan
[b] Department of Mathematics and Computer Science, University of Larbi Ben M'hidi, Oum El Bouaghi, 04000, Algeria
[c] Dipartimento Ingegneria Innovazione, Universita del Salento, Lecce, 73100, Italy

ARTICLE INFO

Keywords:
Fractional discrete *SEIR* model
COVID-19
Chaotic dynamics
Stability

ABSTRACT

This study aims to generalize the discrete integer-order SEIR model to obtain the novel discrete fractional-order SEIR model of COVID-19 and study its dynamic characteristics. Here, we determine the equilibrium points of the model and discuss the stability analysis of these points in detail. Then, the non-linear dynamic behaviors of the suggested discrete fractional model for commensurate and incommensurate fractional orders are investigated through several numerical techniques, including maximum Lyapunov exponents, phase attractors, bifurcation diagrams and C_0 algorithm. Finally, we fitted the model with actual data to verify the accuracy of our mathematical study of the stability of the fractional discrete COVID-19 model.

Introduction

The Coronavirus Pandemic (COVID-19) is an infectious sickness that is highly contagious caused by the severe acute respiratory syndrome coronavirus 2 (SARS-CoV-2 virus). In December 2019, Wuhan, China, became the first city to report an outbreak of COVID-19. The World Health Organization (WHO) declared in early 2020 that the epidemic had spread throughout the globe, creating a worldwide public health emergency. Since then, more than 450 million people have been reported to be infected with the COVID-19 virus, with over 6 million deaths [1,2]. In most cases, the virus is communicated via the air, and a person may get the illness by inhaling air that has been contaminated by the virus-containing nose and mouth spray droplets [3]. The elderly and those suffering from chronic illnesses such as obesity, diabetes, respiratory issues, cardiovascular disease, and other conditions are the most vulnerable [4,5]. In response to the rapid spread of the COVID-19 outbreak, governments have implemented a variety of methods to contain it, such as social distancing, isolation of infected individuals, partial and complete lockdowns of some facilities, and other measures. These policies had a major negative impact on economic development and growth. Therefore, in an attempt to promote the economy, several governments have eased these measures. As a result, the outbreak has not yet been brought fully under control. In order to limit the spread of COVID-19 and immunize the population, several laboratories have developed some vaccines, and some of these vaccines are approved for use. Vaccination is an essential tool in the control and mitigation of epidemic disease outbreaks. According to official World Health Organization statistics, more than 10.5 billion doses of vaccine have been administered globally to date [6].

Fractional calculus is a significant tool for mathematical modeling of numerous issues in physics and mathematics. Discrete fractional calculus has drawn the interest of a great number of researchers during the last several years [7], and they have been increasingly interested in its potential applications in neural networks, secure communication, biology, and other domains. Recently, numerous different dynamics, including chaos, hyperchaos and coexisting attractors in fractional-order systems, have been explored [8–11]. For example, the hyperchaotic dynamics of the fractional generalized H'enon map have been analyzed [12]. In [13], a 3D fractional iterated map has been developed, in which this fractional map was shown to have hidden attractors whereas, the chaos in the fractional Hénon-Lozi type map has been examined in [14]. The authors in [15] exhibited the rich chaotic behaviors of a new fractional-order map with an infinite line of equilibria, while In [16], Khennaoui et al. investigated the chaotic dynamics and combined synchronization of three two-dimensional maps. Because of these distinguishing characteristics, fractional-order iterated maps have been extensively researched in a variety of academic domains.

Researchers in the field of epidemiology have widely used fractional-order operators [17–20]. Recent studies have focused on the emergence of the COVID-19 pandemic, where it has garnered considerable interest recently. The authors of [21] developed a mathematical model for COVID-19 that took into consideration both asymptomatic and

* Corresponding author.
E-mail address: abder.abbes@gmail.com (A. Abbes).

https://doi.org/10.1016/j.rinp.2022.105797
Received 22 March 2022; Received in revised form 27 June 2022; Accepted 4 July 2022
Available online 6 July 2022
2211-3797/© 2022 The Author(s). Published by Elsevier B.V. This is an open access article under the CC BY license (http://creativecommons.org/licenses/by/4.0/).

symptomatic groups with diminishing immunity. Fractional derivatives were used to show the behavior of the model of COVID-19 in [22]. Ogunrinde et al. studied the dynamic model of COVID-19 and citizens' reaction [23], while the complex dynamics of a fractional SIR system in the context of COVID-19 has been discussed by Majee et al. in [24]. In [25], the authors presented a SEIRP model of COVID-19 based on Caputo fractional derivative, whereas Kottakkaran et al. examined the SIRD model of COVID-19 based on real data [26]. In addition, the dynamical of a novel discrete fractional SITR COVID-19 model was analyzed in [27]. Further mathematical models connected to the COVID-19 pandemic may be found [28–31].

In this research, we reformulate a new fractional discrete SEIR model by using the Caputo fractional difference operator, then we examine the model's dynamics and analyze the stability of the equilibrium points of the system at different fractional values in detail by using theoretical and numerical techniques. In addition, we will use COVID-19 data from the United Kingdom and Italy in this model to verify the accuracy of our mathematical study. The work is structured as follows: The SEIR mathematical model for COVID-19 and some basic preliminaries to discrete fractional calculus are presented in Section "The SEIR fractional-order discrete model". In Section "Stability analysis", the fixed points and their regions of stability are explored in detail. The non-linear dynamic behaviors of the suggested discrete fractional model and the C_0 complexity algorithm for commensurate and incommensurate fractional orders are investigated in Section "Nonlinear dynamics of the COVID-19 model". Finally, Section "Discussion" fitted the model with real data obtained from two nations, the United Kingdom and Italy, to verify the accuracy of our mathematical study of the stability of the fractional discrete COVID-19 model.

The SEIR fractional-order discrete model

In this section, we will present the $SEIR$ discrete model proposed in [32], which consists of susceptible group S, infected group I, exposed group E and recovered group R. The model's structure as well as the transmissions between its groups have been depicted in Fig. 1. The $SEIR$ model can be described as follows:

$$\begin{cases} S_{m+1} = \lambda + (1-\mu)S_m - \beta_1\ S_m E_m - \beta_2\ S_m\ I_m + \tau R_m, \\ E_{m+1} = \beta_1\ S_m\ E_m + \beta_2\ S_m\ I_m + (1-\mu-\phi)E_m, \\ I_{m+1} = \phi\ E_m + (1-\mu-\eta)I_m, \\ R_{m+1} = \eta\ I_m - (\mu+\tau)R_m, \end{cases} \tag{1}$$

β_1 and β_2 are referred to as infection rates, and they are defined by $\beta_1 = \frac{\rho_1\kappa_1}{N}$ and $\beta_2 = \frac{\rho_2\kappa_2}{N}$, where ρ_i and κ_i $(j = 1,2)$ represent the probabilities of spreading the disease and the average contacts of each person, respectively, and N represents the total population $(N = S + E + I + R)$. λ denotes the recruitment rate to the susceptible group and μ is the natural disease death rate. η represents the recovering rate of the infected group, ϕ represents the rate of transmission from the exposed group to the infected group, and τ represents the rate of transmission from the recovered group from infection to the susceptible group.

Now, assume that the infection rate $\beta = \beta_1 = \beta_2$ and according to $N = \frac{\lambda}{\mu}$, the $SEIR$ discrete model (1) may be simplified to the following three-dimensional equivalent system:

$$\begin{cases} S_{m+1} = \lambda\ \left(1+\frac{\tau}{\mu}\right) + (1-\tau-\mu)\ S_m - \beta\left(S_m\ E_m + S_m\ I_m\right) - \tau\left(I_m + E_m\right), \\ E_{m+1} = \beta\left(S_m\ E_m + S_m\ I_m\right) + (1-\mu-\phi)\,E_m, \\ I_{m+1} = \phi\ E_m + (1-\mu-\eta)\,I_m. \end{cases} \tag{2}$$

The new fractional discrete-time COVID-19 model is obtained by using the Caputo-like difference operator ${}^{C}\Delta_0^{\gamma_i}$:

$$\begin{cases} {}^{C}\Delta_0^{\gamma_1} S(\nu) = \lambda\left(1+\frac{\tau}{\mu}\right) - (\tau+\mu)\,S\left(\nu-1+\gamma_1\right) \\ \qquad\qquad - \beta\left(\ S\left(\nu-1+\gamma_1\right) E\left(\nu-1+\gamma_1\right) \right. \\ \qquad\qquad \left. + S\left(\nu-1+\gamma_1\right) I\left(\nu-1+\gamma_1\right)\ \right) \\ \qquad\qquad - \tau\Big(I\left(\nu-1+\gamma_1\right) + E\left(\nu-1+\gamma_1\right)\Big), \\ {}^{C}\Delta_0^{\gamma_2} E(\nu) = \beta\left(\ S\left(\nu-1+\gamma_2\right) E\left(\nu-1+\gamma_2\right)\right. \\ \qquad\qquad \left. + S\left(\nu-1+\gamma_2\right) I\left(\nu-1+\gamma_2\right)\ \right) \\ \qquad\qquad - \ (\mu+\phi)\,E\left(\nu-1+\gamma_2\right), \\ {}^{C}\Delta_0^{\gamma_3} I(\nu) = \phi E\left(\nu-1+\gamma_3\right) - (\mu+\eta)\,I\left(\nu-1+\gamma_3\right), \end{cases} \tag{3}$$

for $\nu \in \mathbb{N}_{1-\gamma}$, where $N_{1-\gamma} = \{1-\gamma, 2-\gamma, 3-\gamma, \ldots\}$, $0 < \gamma_j \le 1, j = 1,2,3$ are the fractional orders. The Caputo-like difference operator ${}^{C}\Delta_0^{\gamma}X(\nu)$ of a function $X(\nu)$ is defined as [33]

$$\begin{aligned} {}^{C}\Delta_0^{\gamma}X(\nu) &= \Delta_0^{-(1-\gamma)}\Delta X(t) \\ &= \frac{1}{\Gamma(1-\gamma)}\sum_{t=0}^{\nu-(1-\gamma)}(\nu-1-t)^{(-\gamma)}\Delta X(t). \end{aligned} \tag{4}$$

$\Delta_0^{-\gamma}$ is the $\gamma - th$ fractional sum which is given by [34]

$$\Delta_o^{-\gamma}X(t) = \frac{1}{\Gamma(\gamma)}\sum_{t=o}^{\nu-\gamma}(\nu-1-t)^{(\gamma-1)}X(t), \tag{5}$$

with $\gamma > 0$. The term $(\nu-1-t)^{(\gamma-1)}$ denotes the falling function which is defined as

$$(\nu-1-t)^{(\gamma-1)} = \frac{\Gamma(\nu-t)}{\Gamma(\nu-t-\gamma+1)}. \tag{6}$$

Stability analysis

Fixed points

To calculate the fixed points of the system, we solve the following system of equations:

$$\lambda\left(1+\frac{\tau}{\mu}\right) - \left(\mu+\tau\right)S - \beta\Big(SE+SI\Big) - \tau\Big(I+E\Big) = 0, \tag{7a}$$

$$\beta\Big(SE+SI\Big) - \Big(\mu+\phi\Big)E = 0, \tag{7b}$$

$$\phi\ E - \Big(\mu+\eta\Big)I = 0. \tag{7c}$$

For $I = 0$, the system has free fixed point $X_0 = (\frac{\lambda}{\mu}, 0, 0)$. Assume $I \neq 0$, then from Eq. (7c), we get:

$$\phi\ \bar{E} - (\mu+\eta)\,\bar{I} = 0,$$

i.e

$$\bar{E} = \frac{\mu+\eta}{\phi}\,\bar{I}. \tag{8}$$

Substitute (8) in (7b), we obtain:

$$\beta\left(\bar{S}\bar{E} + \bar{S}\bar{I}\right) - (\mu+\phi)\,\bar{E} = 0,$$

i.e

$$\beta\left(\frac{\mu+\eta+\phi}{\phi}\right)\bar{S}\bar{I} - \frac{(\mu+\phi)(\mu+\eta)}{\phi}\bar{I} = 0,$$

i.e

$$\bar{S} = \frac{(\mu+\phi)(\mu+\eta)}{\beta(\mu+\eta+\phi)}. \tag{9}$$

By replacing (8) and (9) in Eq. (7a), we find

$$\lambda\left(1+\frac{\tau}{\mu}\right) - (\mu+\tau)\,\bar{S} - \beta\left(\bar{S}\bar{E} + \bar{S}\bar{I}\right) - \tau\left(\bar{I}+\bar{E}\right) = 0,$$

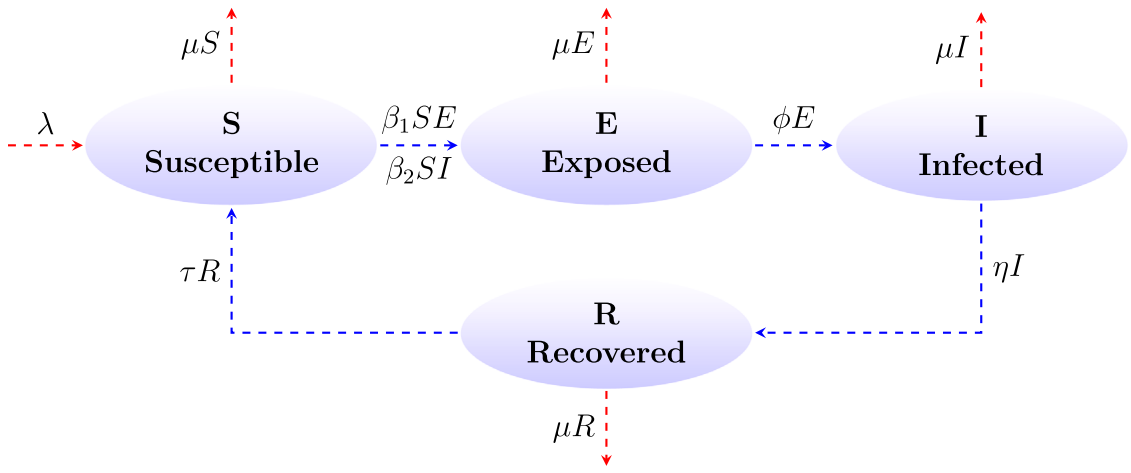

Fig. 1. Structure of the discrete SEIR model.

i.e

$$\left(\frac{\mu+\tau}{\mu}\right)\left(\lambda-\frac{\mu(\mu+\phi)(\mu+\eta)}{\beta(\mu+\eta+\phi)}\right)-\frac{(\mu+\phi)(\mu+\eta)}{\phi}\bar{I}-\frac{\tau}{\phi}(\phi+\mu+\eta)\bar{I}=0,$$

i.e

$$\bar{I}=\left(\frac{\phi(\mu+\tau)}{\mu}\right)\left(\frac{\lambda-\frac{\mu(\mu+\phi)(\mu+\eta)}{\beta(\mu+\eta+\phi)}}{(\mu+\phi)(\mu+\eta)+\tau(\phi+\mu+\eta)}\right),$$

$$=\left(\frac{\phi(\mu+\tau)(\mu+\phi)(\mu+\eta)}{\beta\left(\mu+\eta+\phi\right)}\right)\left(\frac{\frac{\lambda\beta(\mu+\eta+\phi)}{\mu(\mu+\phi)(\mu+\eta)}-1}{(\mu+\phi)(\mu+\eta)+\tau(\phi+\mu+\eta)}\right).$$

Thus, the endemic fixed point $X_1=(S_2,E_2,I_2)$, is given by:

$S_2=\frac{(\mu+\phi)(\mu+\eta)}{\beta(\mu+\eta+\phi)}$.

$E_2=\frac{\mu+\eta}{\phi}I_2$.

$I_2=\frac{\phi(\mu+\tau)(\mu+\phi)(\mu+\eta)(R_0-1)}{\beta(\mu+\eta+\phi)((\mu+\phi)(\mu+\eta)+\tau(\phi+\mu+\eta))}$.

R_0 denotes the reproduction number of the system which is described as the spectral radius of the matrix WG^{-1} [35], where W and G are given as:

$$W=\begin{pmatrix}\beta\frac{\lambda}{\mu} & \beta\frac{\lambda}{\mu}\\ 0 & 0\end{pmatrix}\quad\text{and}\quad G=\begin{pmatrix}\phi+\mu & 0\\ -\phi & \eta+\mu\end{pmatrix},$$

the inverse of G is

$$G^{-1}=\begin{pmatrix}\frac{1}{\phi+\mu} & 0\\ \frac{\phi}{(\phi+\mu)(\eta+\mu)} & \frac{1}{\eta+\mu}\end{pmatrix},$$

so

$$WG^{-1}=\begin{pmatrix}\frac{\beta\lambda(\mu+\eta+\phi)}{\mu(\mu+\phi)(\mu+\eta)} & \frac{\beta\lambda}{\mu(\mu+\eta)}\\ 0 & 0\end{pmatrix}.$$

Thus, by calculating the eigenvalues of the matrix WG^{-1}, we get the reproduction number:

$$R_0=\frac{\beta\lambda(\mu+\eta+\phi)}{\mu(\mu+\phi)(\mu+\eta)}.$$

Note that if $R_0<1$, then the system has only disease free fixed point X_1 and if $R_0>1$, then the system has also unique endemic fixed point X_2.

Stability of the fixed points

In order to determine the conditions of stability for the fixed points of a discrete fractional system, it is necessary to recall the following theorem [36]:

Theorem 1. *Let $g(\nu)=(g_1(\nu),\dots,g_m(\nu))^T$, $0<\gamma<1$ be a fractional order and $B\in\mathbb{R}^{m\times m}$. The zero equilibrium point of the commensurate discrete fractional order system*

$$^{C}\Delta_{\theta}^{\gamma}g(\nu)=B\ g(\nu-1+\gamma), \tag{10}$$

$\forall\ \nu\in\mathbb{N}_{\theta+1-\gamma}$ is asymptotically stable if

$$\lambda_j\in\left\{\xi\in\mathbb{C}:|\xi|\le\left(2\cos\frac{|\arg\xi|-\pi}{2-\gamma}\right)^{\gamma}\quad\text{and}\quad|\arg\xi|\ge\frac{\gamma\,\pi}{2}\right\}, \tag{11}$$

where λ_j are the eigenvalues of the matrix B.

Now, we analyze the stability conditions of the fixed point X_0 as follows

Theorem 2. *The fixed point X_0 of the fractional model (3) is asymptotically stable if either one of the following two sets of conditions are satisfied*

$|\mu+\tau|<2^{\gamma},\quad D\ge 0,\quad C>\sqrt{D},\quad|\frac{-C\pm\sqrt{D}}{2\mu}|<2^{\gamma},$

where $C=\phi\mu+\eta\mu+2\mu^2-\beta\lambda,\quad D=\beta^2\lambda^2+2\beta\phi\lambda\mu+2\beta\eta\lambda\mu+\mu^2(\phi+\eta)^2$.

or

$|\mu+\tau|<2^{\gamma},\quad D<0,\quad|\arg\xi_{2,3}|>\frac{\pi\gamma}{2},\quad|\xi_{2,3}|<\left(2\cos\frac{|\arg\xi_{2,3}|-\pi}{2-\gamma}\right)^{\gamma}.$

$\xi_{2,3}=\frac{-(\phi\mu+\eta\mu+2\mu^2-\beta\lambda)\pm\sqrt{\beta^2\lambda^2+2\beta\phi\lambda\mu+2\beta\eta\lambda\mu+\mu^2(\phi-\eta)^2}}{2\mu}$.

Proof. The Jacobian matrix of the fractional system (3) may be obtained at the fixed point X_0 as follow:

$$J=\begin{pmatrix}-\mu-\tau & -\beta\frac{\lambda}{\mu}-\tau & -\beta\frac{\lambda}{\mu}-\tau\\ 0 & \beta\frac{\lambda}{\mu}-\phi-\mu & \beta\frac{\lambda}{\mu}\\ 0 & \phi & -\eta-\mu\end{pmatrix},$$

then the eigenvalues of J are given by

$\xi_1=-\mu-\tau$,

$\xi_{2,3}=\frac{-(\phi\mu+\eta\mu+2\mu^2-\beta\lambda)\pm\sqrt{\beta^2\lambda^2+2\beta\phi\lambda\mu+2\beta\eta\lambda\mu+\mu^2(\phi-\eta)^2}}{2\mu}$.

Therefore, the argument of the eigenvalue ξ_1 is π which satisfy $|\arg\xi_1|=\pi\ge\frac{\gamma\,\pi}{2}$. The condition $|\xi_1|\le\left(2\cos\frac{|\arg\xi_1|-\pi}{2-\gamma}\right)^{\gamma}=2^{\gamma}$ is satisfied if $|\mu+\tau|<2^{\gamma}$.

Now, for $\beta^2\lambda^2+2\beta\phi\lambda\mu+2\beta\eta\lambda\mu+\mu^2(\phi+\eta)^2\ge 0$, the arguments of the eigenvalues $\xi_{2,3}$ are π if $\xi_{2,3}<0$ i.e,:

$$-(\phi\mu+\eta\mu+2\mu^2-\beta\lambda)>\sqrt{\beta^2\lambda^2+2\beta\phi\lambda\mu+2\beta\eta\lambda\mu+\mu^2(\phi+\eta)^2}.$$

Hence, $|\arg\xi_{2,3}|=\pi\ge\frac{\gamma\,\pi}{2}$. For the second condition of the theorem, we have $|\xi_{2,3}|\le\left(2\cos\frac{|\arg\xi_{2,3}|-\pi}{2-\gamma}\right)^{\gamma}=2^{\gamma}$ which implies $|\frac{-C\pm\sqrt{D}}{2\mu}|<2^{\gamma}$, where $C=\phi\mu+\eta\mu+2\mu^2-\beta\lambda$ and $D=\beta^2\lambda^2+2\beta\phi\lambda\mu+2\beta\eta\lambda\mu+\mu^2(\phi+\eta)^2$.

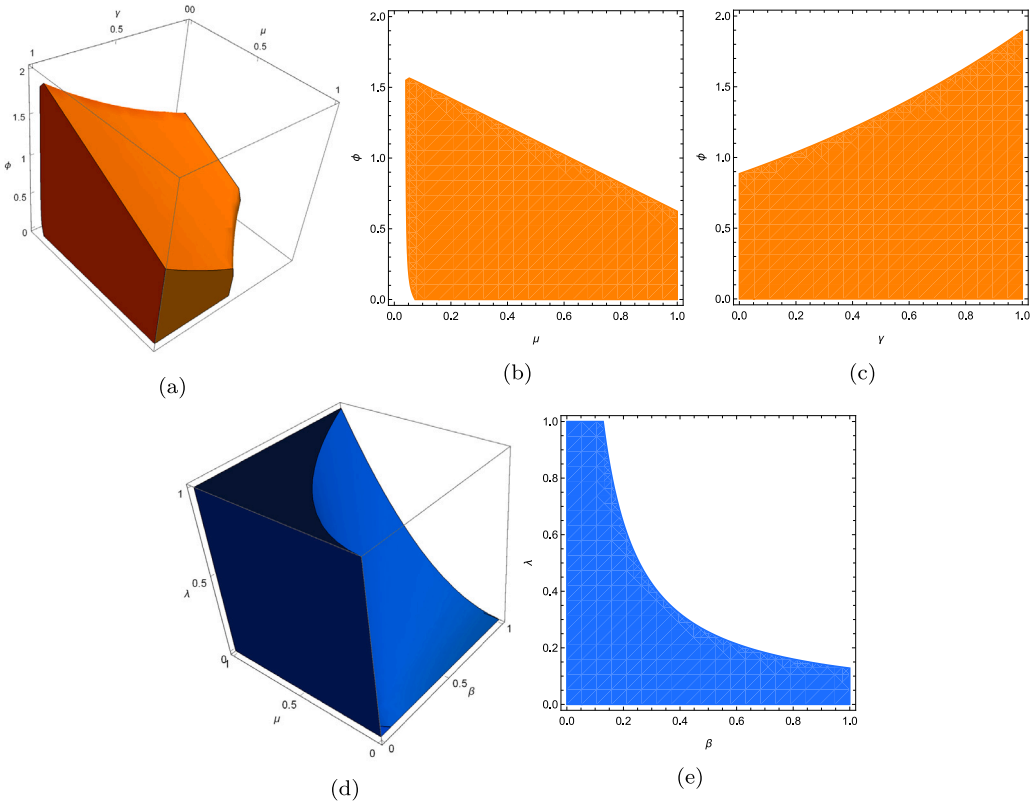

Fig. 2. Stability region of the fixed point X_0 for $\tau = 0.4$, $\beta = 0.018$, $\eta = 0.2$ in (a) $\gamma - \mu - \phi$ space, (b) $\mu - \phi$ plane for $\gamma = 0.7$, (c) $\gamma - \phi$ plane for $\mu = 0.1$, (d) $\beta - \mu - \lambda$ space, (e) $\beta - \lambda$ plane for $\mu = 0.35$ and $\gamma = 0.7$.

The eigenvalues take complex values if $\beta^2\lambda^2+2\beta\phi\lambda\mu+2\beta\eta\lambda\mu+\mu^2(\phi+\eta)^2 < 0$. The stability conditions is satisfied if

$$|\arg \xi_{2,3}| > \frac{\pi\gamma}{2}, \quad |\xi_{2,3}| < \left(2\cos\frac{|\arg \xi_{2,3}| - \pi}{2-\gamma}\right)^{\gamma},$$

and thus the proof is complete.

Given the complex expression of the endemic equilibrium point X_1, the stability regions of this point will be explored using large-scale numerical simulations in parameter spaces of the model.

The stability regions of the fixed points

This section will investigate the influence of the parameters in the COVID-19 system (3) on the stability of the fixed points. The stability areas of fixed points are investigated in accordance with the conditions of stability that were previously established. Fig. 2(a) displays the stability region of the free fixed point X_0 in $(\gamma - \phi - \mu)$ space, while Figs. 2(b) and 2(c) show the stability region of X_0 in the $(\mu - \phi)$ plane for $\gamma = 0.7$ and in the $(\gamma - \phi)$ plane for $\mu = 0.1$, respectively. It can be seen that the stability region of the fixed point decreases as the natural death rate μ increases or when the fractional order γ approaches zero. Fig. 2(d) illustrates the area of stability of X_0 in space $(\beta - \lambda - \mu)$ and Fig. 2(e) shows the stability region of X_0 in the plane $(\beta-\lambda)$. Notice that changing the value of the infection rate β has the effect of expanding or contracting the region in which X_0 is stable. Now, in order to show the influence of the parameter μ and the fractional order γ on the stability of X_0, Fig. 3(a) depicts the stability region in $(\gamma - \eta - \phi)$ space for $\mu = 0.1$. Figs. 3(b) and 3(c) depict the stability regions in $(\eta - \phi)$ two-dimensional plan for $\mu = 0.1$, $\gamma = 0.1$ (Fig. 3(b)), and $\gamma = 0.4$ (Fig. 3(c)). Similarly, assume that the natural death rate increased to $\mu = 0.35$ and then evaluate stability areas in the same preceding parameters spaces (see Figs. 3(d)–3(f)). It is clear that the increase in μ or the decrease of the fractional order γ led to a rise in the size of the stability region of the fixed point X_0.

Furthermore, we investigate the stability of the fixed point X_1. Fig. 4(a) depicts the region of stability of X_1 in $(\beta - \gamma - \mu)$ space, while Fig. 4(b) investigates the region of stability of X_1 in the $(\beta - \mu)$ plane for $\gamma = 0.7$. It can be shown that the stability region of X_0 shrinks as the values of β and μ approach 0. Now, we illustrate the stability area of X_1 in both $(\beta - \eta - \mu)$ space and the $(\eta - \beta)$ plane. From Figs. 4(c) and 4(d), it is shown that as η increases, the stability region shrinks and the fixed point becomes unstable. Fig. 4(e) depicts the region of stability for $\gamma = 0.4$. Clearly, increasing the value of the fractional-order made the fixed point X_1 more stable. Time evolutions of the states of the system (3) are obtained at various parameter values to verify the aforementioned findings. Examples of where the free-disease fixed point X_0 is stable are illustrated in Figs. 5(a) and 5(b). In addition, two cases in which the endemic fixed point X_1 is stable are shown in Figs. 5(c) and 5(d).

Nonlinear dynamics of the COVID-19 model

In this part, we will investigate the chaotic behavior of the proposed discrete fractional COVID-19 model (3). This investigation will be carried out using a variety of numerical methods, including Lyapunov exponent calculations, bifurcation diagrams, and the display of phase portraits. Also, we apply the C_0 algorithm to measure the complexity of the system. First, we will offer the following theorem, which will allow us to construct the numerical formula for the fractional discrete model. In order to explore the dynamical characteristics that may be seen in the discrete fractional system (3), we will need to use this formula.

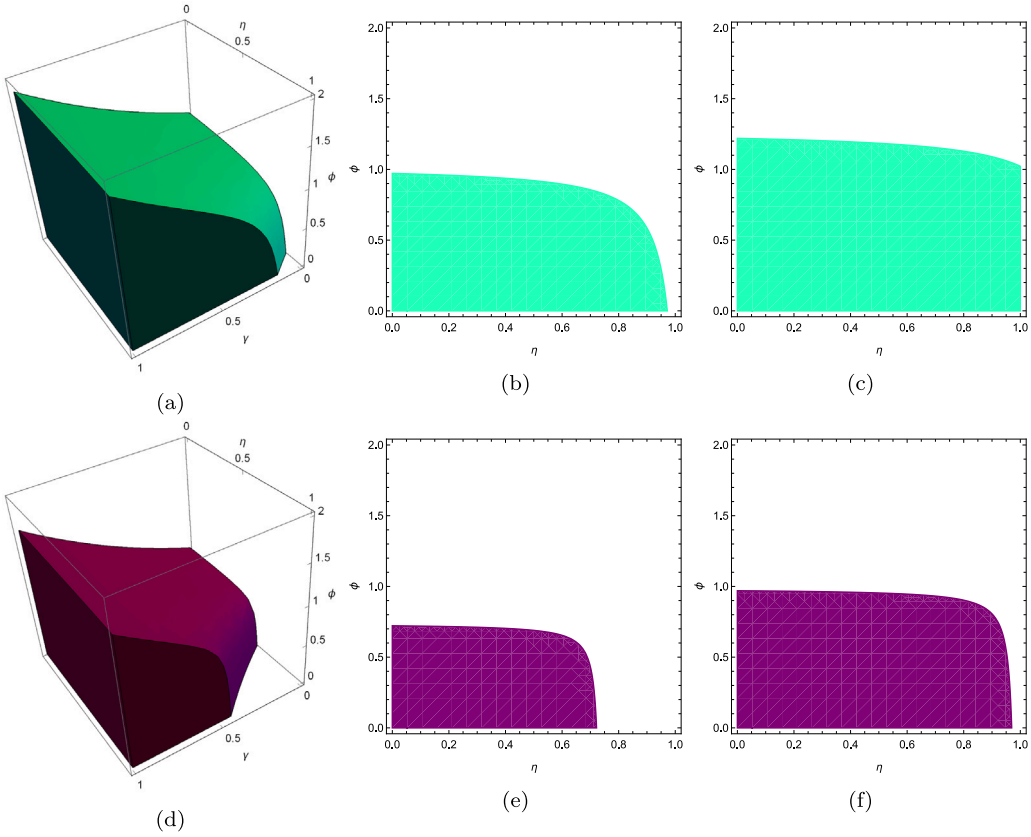

Fig. 3. Stability region of the fixed point X_0 for $\tau = 0.4$, $\beta = 0.018$, $\lambda = 0.3$ in (a) $\gamma - \eta - \phi$ space for $\mu = 0.1$ (b) $\eta - \phi$ plane for $\gamma = 0.1$ (c) $\eta - \phi$ plane for $\gamma = 0.4$ (d) $\gamma - \eta - \phi$ space for $\mu = 0.35$ (e) $\eta - \phi$ plane for $\gamma = 0.1$ (f) $\eta - \phi$ plane for $\gamma = 0.4$.

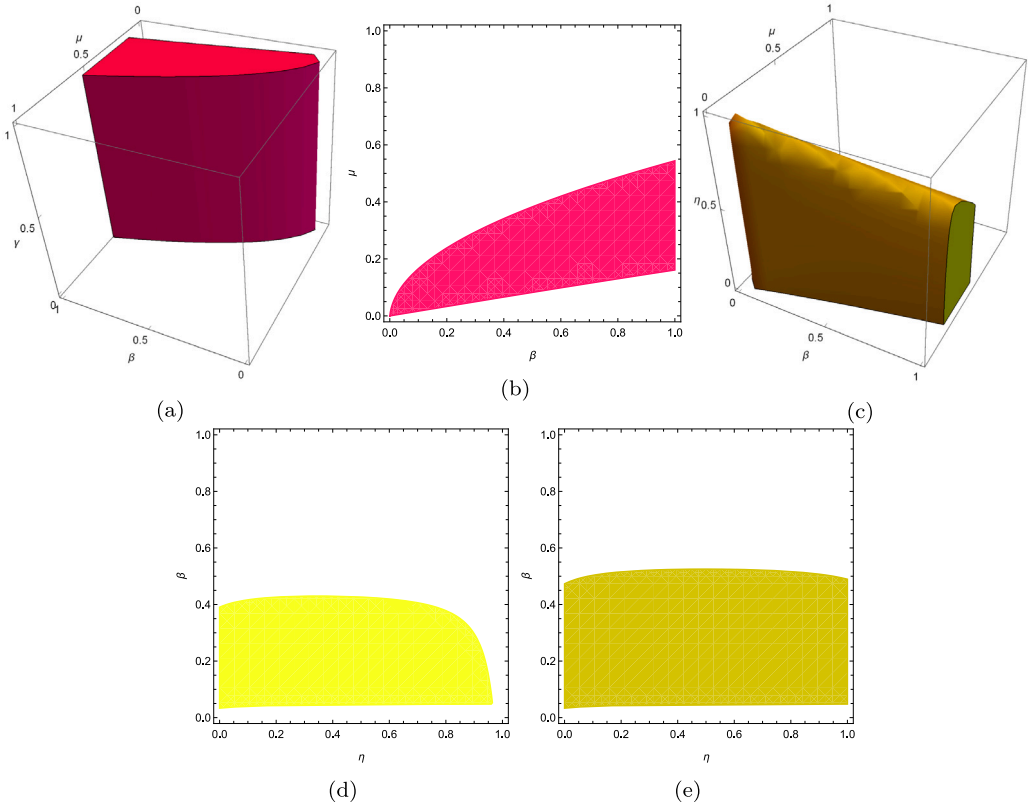

Fig. 4. Stability region of the fixed point X_1 for $\tau = 0.4$, $\phi = 0.05$, $\lambda = 0.3$ in (a) $\beta - \gamma - \mu$ space (b) $\beta - \mu$ plane for $\gamma = 0.7$ (c) $\beta - \eta - \mu$ space for $\gamma = 0.1$ (d) $\beta - \eta$ space for $\mu = 0.1$ and $\gamma = 0.1$ (e) $\beta - \eta$ plane for $\gamma = 0.4$.

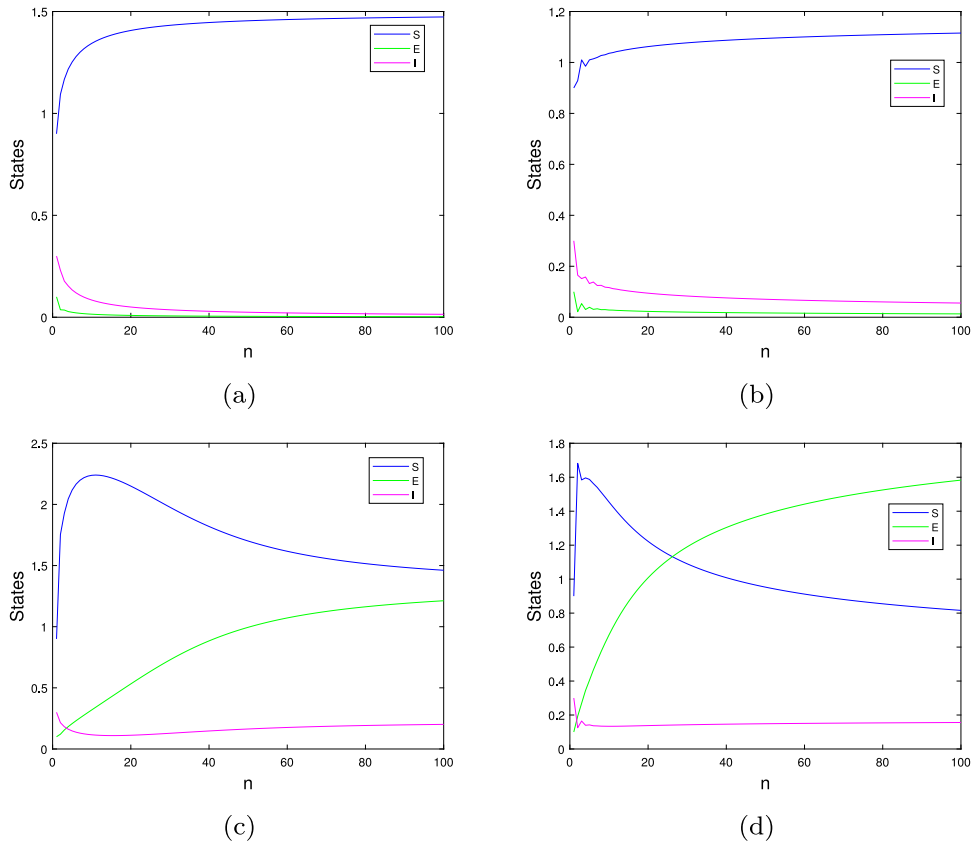

Fig. 5. Time series of states of the $SEIR$ model (3) for (a) $\tau = 0.4,\ \phi = 0.5,\ \lambda = 0.3,\ \beta = 0.018,\ \mu = 0.2.\ \eta = 0.2,\ \gamma = 0.7$ (b) $\tau = 0.4,\ \phi = 0.6,\ \lambda = 0.3,\ \beta = 0.018,\ \mu = 0.25.\ \eta = 0.4,\ \gamma = 0.4$ (c) $\tau = 0.4,\ \phi = 0.05,\ \lambda = 0.3,\ \beta = 0.1,\ \mu = 0.1.\ \eta = 0.2,\ \gamma = 0.7$ (d) $\tau = 0.4,\ \phi = 0.05,\ \lambda = 0.3,\ \beta = 0.3,\ \mu = 0.1.\ \eta = 0.5,\ \gamma = 0.4$.

Theorem 3 ([37]). *For the fractional difference equation*

$$\begin{cases} {}^{C}\Delta_0^{\gamma_j} z(\nu) = h(\nu+\gamma_j-1, z(\nu+\gamma_i-1)), \\ \Delta^{\kappa} z(\nu) = z_{\kappa}, \quad m = \lceil \gamma_j \rceil + 1, \end{cases} \tag{12}$$

the unique solution of this initial value problem (12) is given by

$$z(\nu) = z_0(\nu) + \frac{1}{\Gamma(\gamma_j)} \sum_{\tau=m-\gamma_j}^{\nu-\gamma_j} (\nu-\tau+1)^{(\gamma_j-1)} h(\tau+\gamma_j-1, z(\tau+\gamma_i-1)), \quad \nu \in \mathbb{N}_m, \tag{13}$$

where

$$z_0(\nu) = \sum_{\kappa=0}^{m-1} \frac{(\nu)^{\kappa}}{\Gamma(\kappa+1)} \Delta^{\kappa} z(0). \tag{14}$$

The numerical formula of the discrete fractional COVID-19 system (3) is constructed according to Theorem 3 as:

$$\begin{cases} S(n) = S(0) + \dfrac{1}{\Gamma(\gamma_1)} \displaystyle\sum_{j=0}^{n-1} \frac{\Gamma(n-j-1+\gamma_1)}{\Gamma(n+1-j-1)} \Big(\lambda\big(1+\frac{\tau}{\mu}\big) - (\mu+\tau) S(j) \\ \qquad\qquad - \beta \big(S(j)E(j) + S(j)I(j) \big) - \tau\big(I(j)+E(j)\big) \Big), \\ E(n) = E(0) + \dfrac{1}{\Gamma(\gamma_2)} \displaystyle\sum_{j=0}^{n-1} \frac{\Gamma(n-j-1+\gamma_2)}{\Gamma(n+1-j-1)} \Big(\beta\big(S(j)E(j) + S(j)I(j)\big) \\ \qquad\qquad - (\mu+\phi) E(j) \Big), \\ I(n) = I(0) + \dfrac{1}{\Gamma(\gamma_3)} \displaystyle\sum_{j=0}^{n-1} \frac{\Gamma(n-j-1+\gamma_3)}{\Gamma(n+1-j-1)} \big(\phi\ E(j) - (\mu+\eta) I(j)\big), \end{cases} \tag{15}$$

where $S(0), E(0)$ and $I(0)$ denote initial conditions. This is a new class of COVID-19 model which hold "memory effects". As one can see from Eq. (15), the states $S(n), E(n)$ and $I(n)$ depends on all past variables $S(0), S(1), \ldots, S(n-1)$, $E(0), E(1), \ldots, E(n-1)$ and $I(0), I(1), \ldots, I(n-1)$.

The commensurate fractional orders

We will evaluate the influence of the fractional-order γ on the behavior of the fractional COVID-19 system (3) where the initial conditions are assigned as $(S(0), E(0), I(0)) = (44, 0.01, 0.21)$. Fig. 6 illustrates phase attractors for different orders of γ. One can see that model (3) exhibits a wide range of dynamical behaviors for a variety of fractional values. Furthermore, we have employed β as a bifurcation parameter to draw the bifurcation diagram, and the findings obtained are given in Fig. 7. It is evident that the model progressively transitions from a periodic state to a chaotic one by means of period-doubling bifurcation. As can be observed, the behavior of the model (3) is affected by the change of the fractional values, as reducing the fractional-order shrinks the interval during which chaos occurs. To illustrate the dynamic behavior more accurately, Fig. 8(a) displays the bifurcation diagram of the commensurate fractional discrete COVID-19 model (3) with γ as an adjustable parameter. We can see that there is chaos in the fractional-discrete COVID-19 model (3) and that the fractional-order influences the system's behavior. When the fractional values γ fall below 0.9073, the states of the system diverge towards infinity. In spite of the fact that bifurcation charts may be useful for detecting chaos in fractional systems, computing or estimating the system's Lyapunov exponent (LE) is generally more practical. It is possible to compute the maximum LEs using a Jacobian matrix technique [38]. The Matlab script was used to compute the MLEs and the obtained results are presented in Fig. 8(b). One can note that the system has negative and positive LEs values,

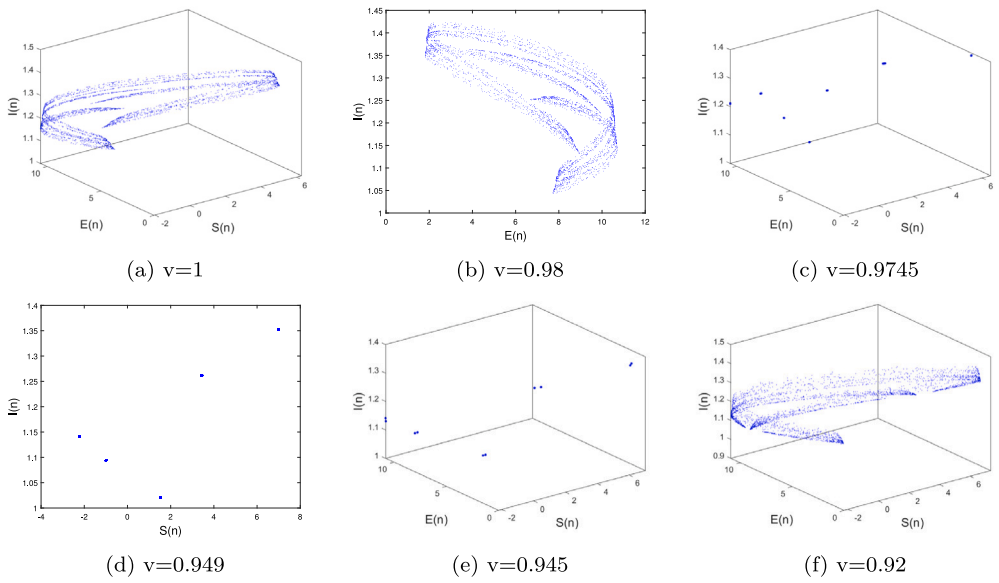

(a) v=1 (b) v=0.98 (c) v=0.9745

(d) v=0.949 (e) v=0.945 (f) v=0.92

Fig. 6. Phase portrait of the fractional discrete COVID-19 system (3) with commensurate fractional order.

meaning that the COVID-19 model (3) transitions from a stable state to a chaotic state, which is consistent with the findings obtained from the bifurcation diagram seen in Fig. 8(a).

The incommensurate fractional orders

Here, we examine the dynamics of the incommensurate fractional discrete COVID-19 model (3) in a manner similar to the case of commensurate orders ($\gamma = (\gamma_1, \gamma_2, \gamma_3)$). In particular, the impact of incommensurate fractional values on the behaviors of the fractional discrete COVID-19 model was investigated by taking γ_1 as the critical parameter for plotting the bifurcation diagram and calculating the maximum LEs. The results are displayed in Fig. 9 for fractional values $\gamma_2 = \gamma_3 = 0.95$ and initial conditions $(S(0), E(0).I(0)) = (44, 0.02, 0.21)$. One can see that the COVID-19 model is chaotic for $\gamma_1 \in [0.937, 0.9455] \cup [0.9505, 0.966] \cup [0.967, 1]$ where the MLEs have positive values. The MLEs change their values between negative and positive when γ_1 decreases, meaning that chaos occurs with the appearance of certain periodic orbits. When γ_1 continues to decrease, the states of the system diverge towards infinity. Furthermore, to assess the dynamical behavior of the fractional COVID-19 system when the fractional order γ_2 changes, Figs. 10(a) and 9(b) illustrate the bifurcation diagram and its corresponding MLEs for $(\gamma_1, \gamma_3) = (1, 0.95)$. We can observe that the behavior of the fractional COVID-19 model (3) has changed from periodic to chaotic when γ_2 increases. This finding confirms that fractional-order γ_2 has a great impact on the dynamics of the states of the system. Additionally, setting fractional values $(\gamma_1, \gamma_2) = (1, 0.95)$ and initial conditions $(S(0), E(0).I(0)) = (44, 0.02, 0.21)$, Fig. 11 shows the bifurcation diagram and the MLEs for $\gamma_3 \in (0, 1]$. The fractional COVID-19 system displays a rather full bifurcation route when γ_3 is utilized as a bifurcation parameter. For $\gamma_3 \in (0, 0.625]$ chaotic behavior can be obtained with positive maximum Lyapunov exponents, while the MLEs have negative values when $\gamma_3 \in]0.625, 0.75]$, so the chaos disappears and periodic windows appear. In addition, when γ_3 gets larger and approaches 1, chaos occurs again. With these results, it is clear that the dynamic behavior of the fractional discrete COVID-19 system with commensurate orders is less complex than the system with incommensurate orders. This also indicates that the system's behavior can be better described by incommensurate orders. For completeness, the phase attractors of the states of the fractional COVID-19 model with incommensurate orders (3) are shown in Fig. 12.

C_0 complexity of the COVID-19 model

According to the inverse Fourier transform, we use the C_0 algorithm to compute the complexity of chaotic models. The algorithm is described as follows [39]: First, the Fourier transform of the series $[S(0), S(1), \ldots, S(N-1)]$ is figured out by

$$Y_N(j) = \frac{1}{N} \sum_{k=0}^{N-1} x(k) \exp^{-2\pi i (\frac{kj}{N})}, \quad j = 0, 1, .., N-1. \tag{16}$$

We calculate the mean square as $G_N = \frac{1}{N} \sum_{j=0}^{N-1} |Y_N(j)|^2$ and we let

$$\bar{Y}_{N(j)} = \begin{cases} Y_N(j) & \text{if} \quad \|Y_N(j)\|^2 > rG_N, \\ 0 & \text{if} \quad \|Y_N(j)\|^2 \leq rG_N. \end{cases} \tag{17}$$

Now, we compute the inverse Fourier transform of $\bar{Y}_N$ as

$$\bar{y}(\kappa) = \frac{1}{N} \sum_{j=0}^{N-1} \bar{Y}_N(j) \exp^{2\pi i (\frac{kj}{N})}, \quad \kappa = 0, 1, .., N-1. \tag{18}$$

Then, we calculate the C_0 complexity as

$$C_0 = \frac{\sum_{\kappa=0}^{N-1} \|\bar{y}(\kappa) - S(\kappa)\|}{\sum_{\kappa=0}^{N-1} \|S(\kappa)\|^2}. \tag{19}$$

The C_0 complexity of the fractional discrete COVID-19 system (3) with fractional order values γ_i varying are computed and the results are presented in Fig. 13. Interestingly, from Fig. 13(a), as with the MLEs, when the commensurate order γ decreases, the C_0 complexity value of the fractional COVID-19 system increases. However, as contrasted to the case of the commensurate fractional model, the incommensurate fractional discrete COVID-19 model (3) exhibits more complexity when the value of γ_2 close to 1. As a result, we can conclude that the C_0 method is an effective tool for measuring complexity accurately. Fig. 13(a) illustrates that the fractional COVID-19 system (3) has higher complexity when $\gamma \in (0.95, 0.966]$. As shown in Fig. 13(c), when

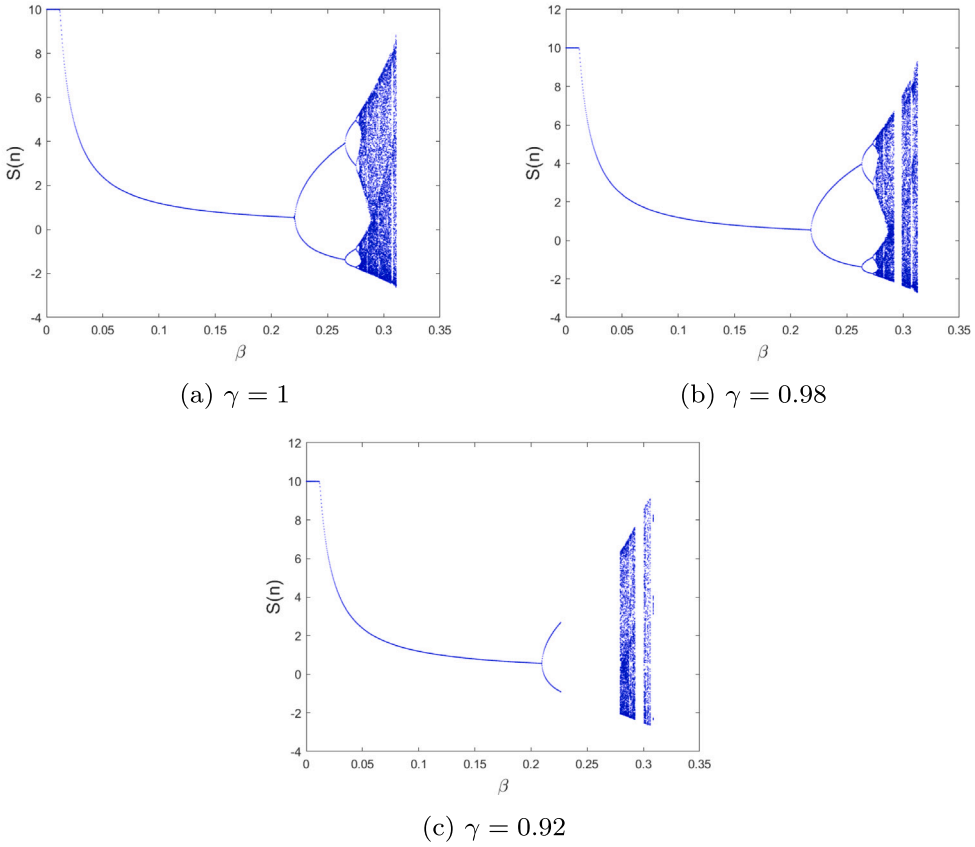

Fig. 7. Bifurcation diagram of the discrete COVID-19 system (3) versus β for $\lambda = 0.9$, $\eta = 0.2$, $\mu = 0.09$, $\tau = 0.8$, $\phi = 0.05$ and (a) $\gamma = 1$, (b) $\gamma = 0.98$, (c) $\gamma = 0.92$.

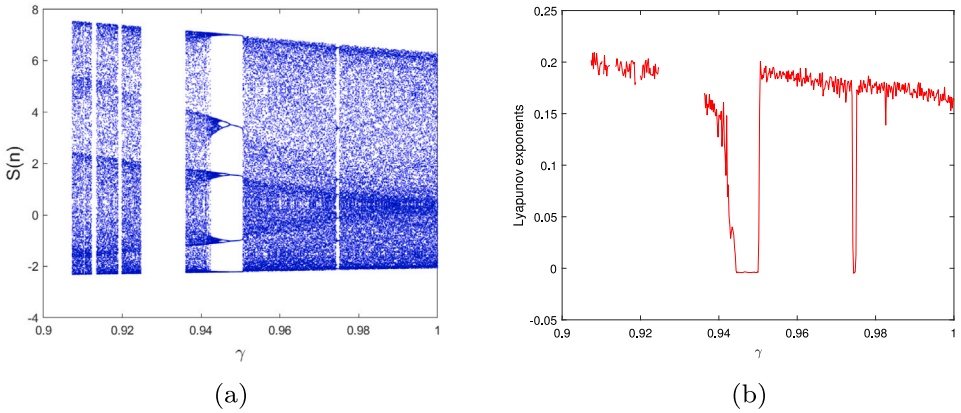

Fig. 8. Bifurcation diagram and Maximum Lyapunov exponents of the fractional discrete COVID-19 system (3) versus γ for $\lambda = 0.9$, $\beta = 0.29$, $\eta = 0.2$, $\mu = 0.09$, $\tau = 0.8$, and $\phi = 0.05$.

$(\gamma_1, \gamma_3) = (1, 0.95)$, the C_0 complexity increase with the increase of fractional value γ_2, and when $(\gamma_1, \gamma_2) = (1, 0.95)$, the C_0 complexity increase with the decrease of fractional value γ_3 (see Fig. 13(c)). These results are consistent with previous results of the MLEs.

Discussion

Finally, we will use published data from two nations, the United Kingdom and Italy, to verify the accuracy of our mathematical study of the stability of the fractional discrete COVID-19 model (3). We fitted the suggested model to the cases of COVID-19 from these nations using the parameters listed in Table 1. Figs. 14 and 15 show the dynamical analysis of the fractional discrete model (3) of the susceptible, exposed, infected, and recovered population for the United Kingdom and Italy. Fig. 14(a) shows that the number of individuals susceptible to the epidemic increases rapidly and then starts decreasing after reaching a peak until it reaches a stable state, while the exposed population increases over time, as depicted in Fig. 14(b). Figs. 14(c) and 14(d) illustrate the scheme of infected and recovered individuals, where we note that the number of infected individuals increases rapidly until it reaches the

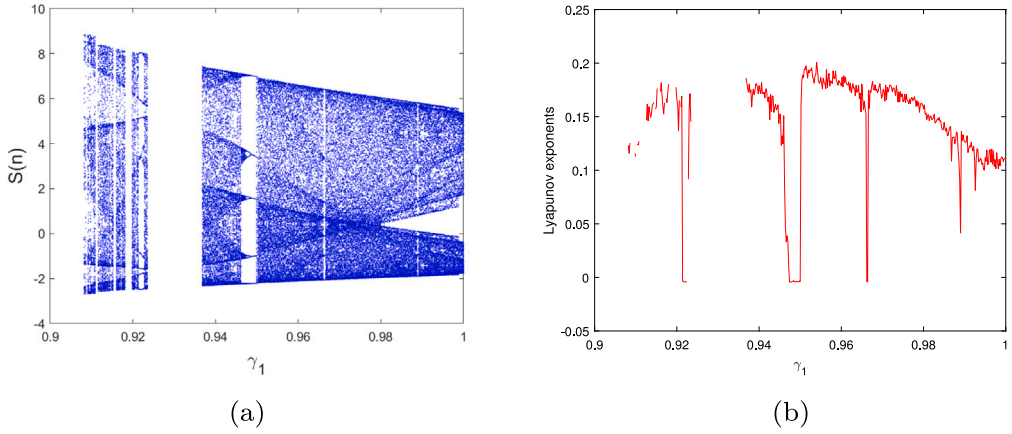

Fig. 9. bifurcation diagram and Maximum Lyapunov exponents of the fractional discrete COVID-19 system (3) versus γ_1 for $\gamma_2 = 0.95$, $\gamma_3 = 0.95$, $\lambda = 0.9$, $\beta = 0.29$, $\eta = 0.2$, $\mu = 0.09$, $\tau = 0.8$, and $\phi = 0.05$.

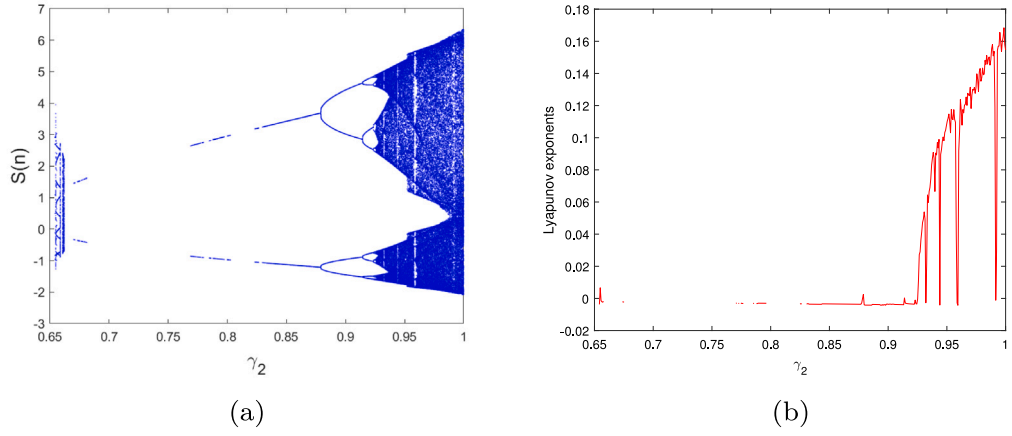

Fig. 10. Bifurcation diagram and Maximum Lyapunov exponents of the fractional discrete COVID-19 system (3) versus γ_2 for $\gamma_1 = 1$, $\gamma_3 = 0.95$, $\lambda = 0.9$, $\beta = 0.29$, $\eta = 0.2$, $\mu = 0.09$, $\tau = 0.8$, and $\phi = 0.05$.

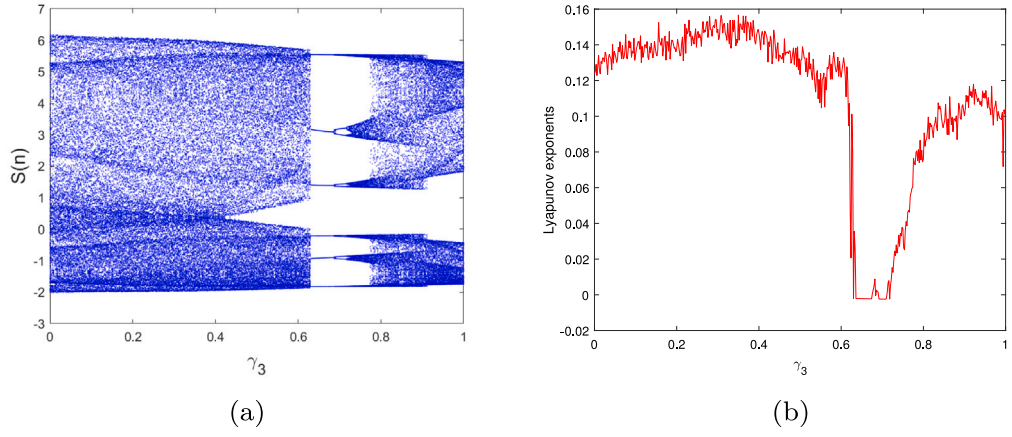

Fig. 11. Bifurcation diagram and Maximum Lyapunov exponents of the fractional discrete COVID-19 system (3) versus γ_3 for $\gamma_1 = 1$, $\gamma_2 = 0.95$, $\lambda = 0.9$, $\beta = 0.29$, $\eta = 0.2$, $\mu = 0.09$, $\tau = 0.8$, and $\phi = 0.05$.

maximum limit, while the number of recovered individuals increases slowly at first, then the number of recovering persons increases gradually over time as a result of using the appropriate treatment medications and starting various vaccination programs. Similarly, we can interpret the results of the real data of the COVID-19 epidemic in Italy depicted in Fig. 15.

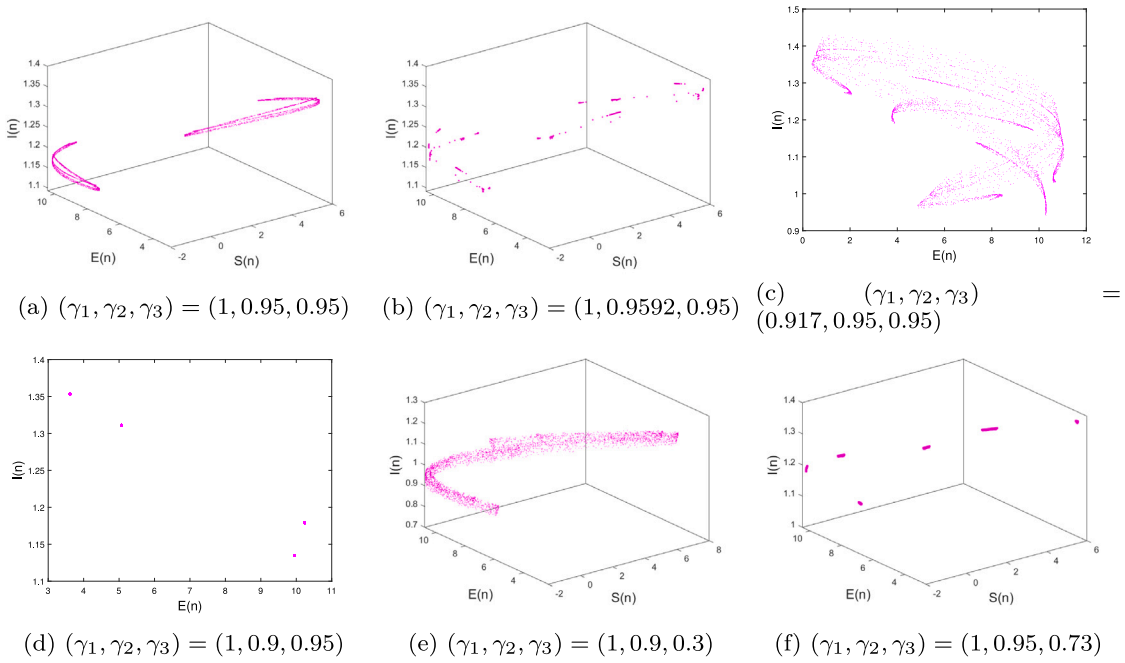

(a) $(\gamma_1, \gamma_2, \gamma_3) = (1, 0.95, 0.95)$ (b) $(\gamma_1, \gamma_2, \gamma_3) = (1, 0.9592, 0.95)$ (c) $(\gamma_1, \gamma_2, \gamma_3) = (0.917, 0.95, 0.95)$

(d) $(\gamma_1, \gamma_2, \gamma_3) = (1, 0.9, 0.95)$ (e) $(\gamma_1, \gamma_2, \gamma_3) = (1, 0.9, 0.3)$ (f) $(\gamma_1, \gamma_2, \gamma_3) = (1, 0.95, 0.73)$

Fig. 12. Phase portrait of the fractional discrete COVID-19 system (3) with incommensurate fractional order.

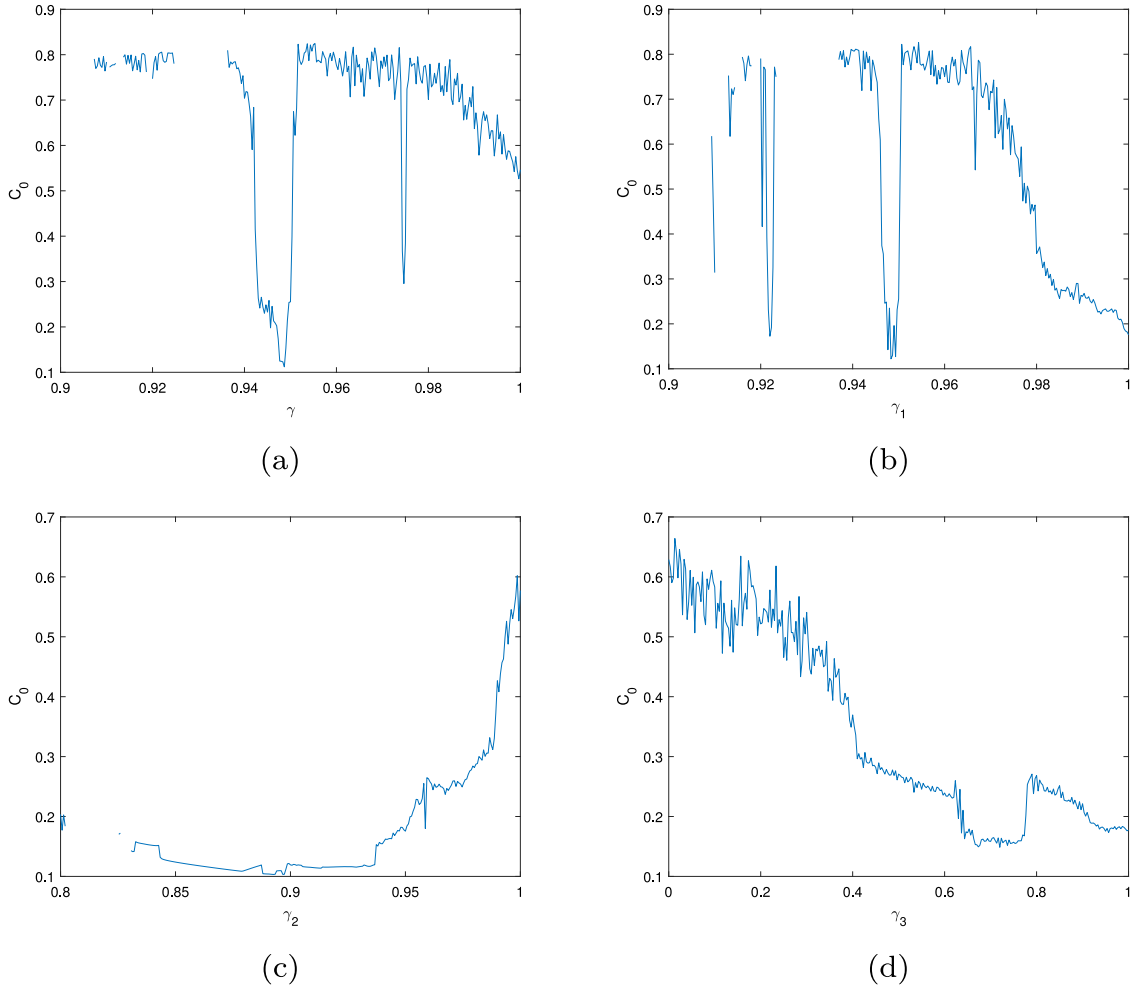

Fig. 13. C_0 complexity analysis of the fractional COVID-19 system (3) for (a) versus γ (b) versus γ_1 with $(\gamma_2, \gamma_3) = (0.95, 0.95)$ (c) versus γ_2 with $(\gamma_1, \gamma_3) = (1, 0.95)$ (d) versus γ_3 with $(\gamma_2 1, \gamma_2) = (1, 0.95)$.

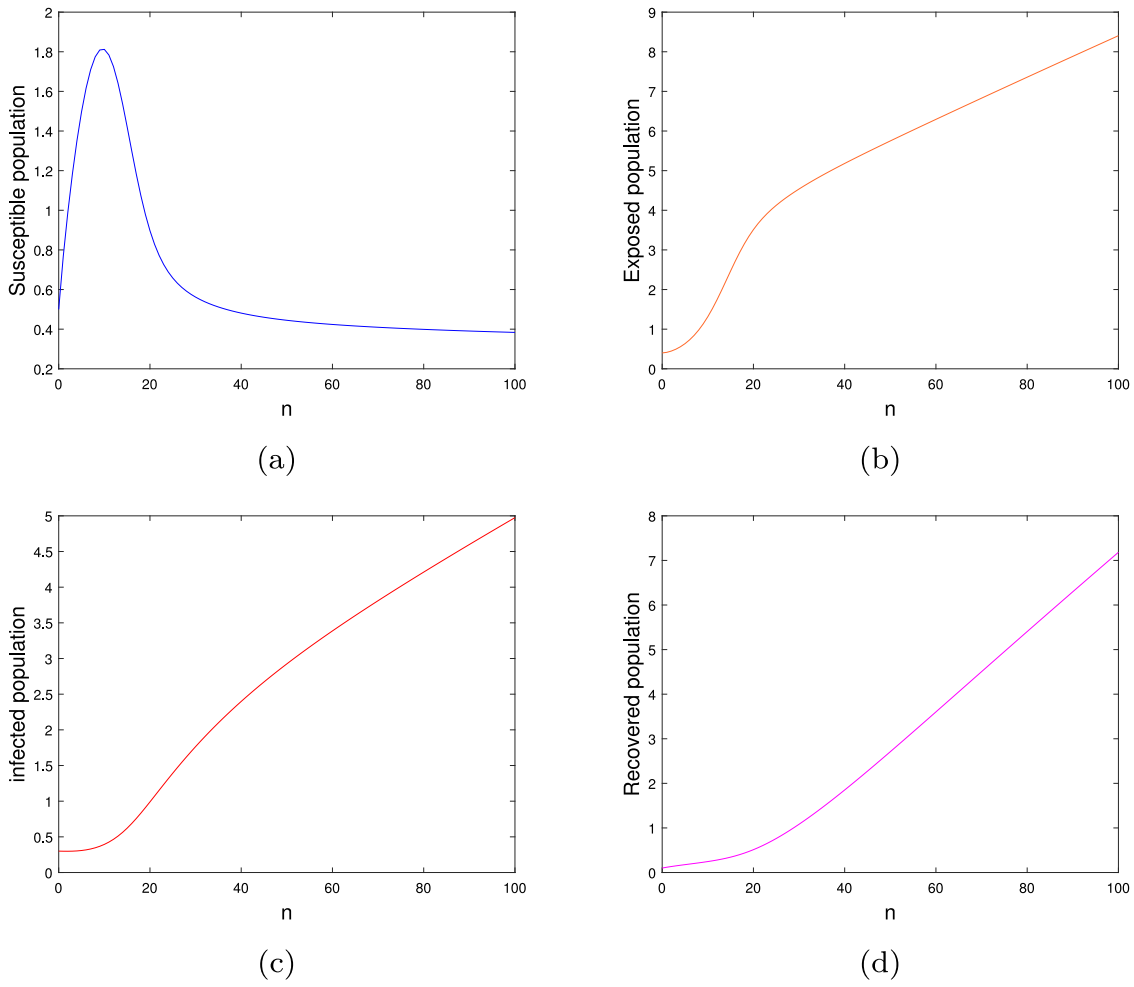

Fig. 14. Evolution of the fractional discrete COVID-19 system (3) in the United Kingdom.

Table 1
Values of parameters in the United Kingdom and Italy.

Parameter	The United Kingdom	Italy	References
λ	0.3	0.3	Estimated
μ	$3.2929 * 10^{-5}$	$3.2612 * 10^{-5}$	[40,41]
β	0.0999	0.0571	[40]
τ	0.0294	0.0338	[42]
γ	0.0714	0.076	[41,43]
ϕ	0.05	0.05	Estimated

Conclusion

In this paper, we proposed a discrete fractional SEIR COVID-19 model depending on the Caputo-like operator. As can be observed, the model involves four variables: susceptible S, exposed E, infected I and recovered R. The non-linear dynamical analysis of the suggested model is carried out in this study as follows: the free-disease fixed point and the endemic fixed point are determined and then studied the conditions of stability of each fixed point. The stability areas for the fixed points are examined in a two-dimensional plane and three-dimensional space. The stability analysis shows that the fractional values, recovering rate and infection rate influenced the stability of the fixed points. The parameter values are chosen in such a manner that they highlight all possible impacts of parameters on the stability of fixed points. The behavior of the discrete fractional SEIR COVID-19 model has been discussed by calculating the maximum Lyapunov exponents and applying the C_0 algorithm for complexity to verify the occurrence of chaos. Real-world data published from the United Kingdom and Italy were also been used in order to confirm the accuracy of our mathematical study of the stability of the suggested model.

CRediT authorship contribution statement

Abderrahmane Abbes: Model investigated and drafted, Investigation, Visualization, Resources, Software, Data curation, Writing – original draft, Writing – review & editing. **Adel Ouannas:** Conceptualization, Methodology, Formally analyzed and viewed with revision, Validation, Visualization, Supervision, Project administration. **Nabil Shawagfeh:** Supervision, Validation, Visualization. **Giuseppe Grassi:** Funding acquisition, Resources.

Declaration of competing interest

The authors declare that they have no known competing financial interests or personal relationships that could have appeared to influence the work reported in this paper.

Data availability

Data will be made available on request.

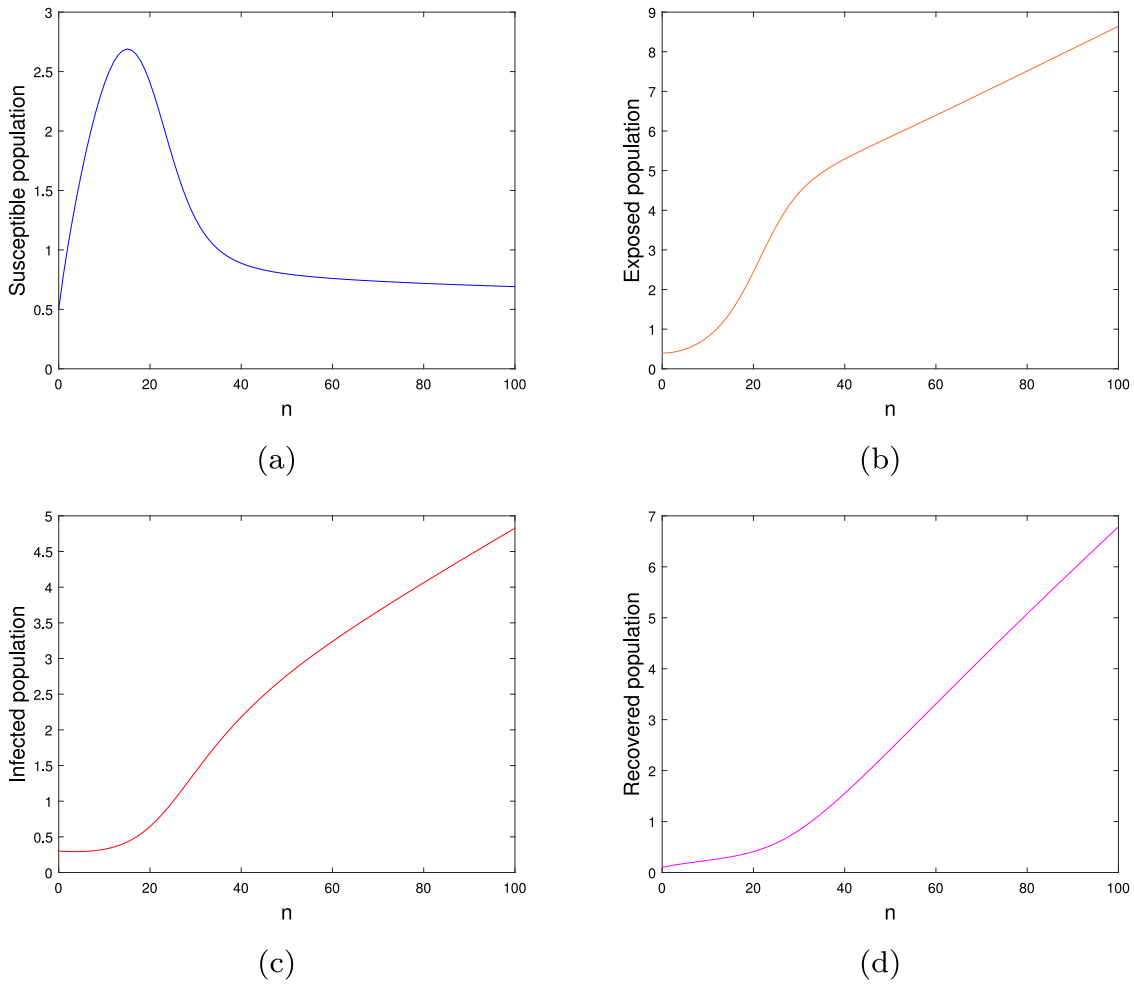

Fig. 15. Evolution of the fractional discrete COVID-19 system (3) in Italy.

References

[1] Worldometers.info. 2022, https://www.worldometers.info/coronavirus/countries-where-coronavirus-has-spread/. [Accessed 5 March 2022].

[2] WHO coronavirus (COVID-19) dashboard, covid19.who.int. 2022, https://covid19.who.int. [Accessed 5 March 2022].

[3] Khan MA, Atangana A. Modeling the dynamics of novel coronavirus (2019-ncov) with fractional derivative. Alex Eng J 2020;59:2379–89. http://dx.doi.org/10.1016/j.aej.2020.02.033.

[4] Rothan HA, Byrareddy SN. The epidemiology and pathogenesis of coronavirus disease (COVID-19) outbreak. J Autoimmun 2020;109:102433. http://dx.doi.org/10.1016/j.jaut.2020.102433.

[5] Bajgain KT, Badal S, Bajgain BB, Santana MJ. Prevalence of comorbidities among individuals with covid-19: A rapid review of current literature. Am J Infec Control 2021;49:238–46. http://dx.doi.org/10.1016/j.ajic.2020.06.213.

[6] COVID-19 vaccines, who.int. 2022, https://www.who.int/emergencies/diseases/novel-coronavirus-2019/covid-19-vaccines. [Accessed 5 March 2022].

[7] Edelman M, Macau E, Sanjuàn M. Chaotic, fractional, and complex dynamics: new insights and perspectives. Cham: Springer International Publishing; 2018.

[8] Peng Y, He S, Sun K. Chaos in the discrete memristor-based system with fractional-order difference. Results Phys 2021;24:104106. http://dx.doi.org/10.1016/j.rinp.2021.104106.

[9] Almatroud AO, Khennaoui AA, Ouannas A, Pham V-T. Infinite line of equilibriums in a novel fractional map with coexisting infinitely many attractors and initial offset boosting. Int J Nonlinear Sci Numer Simul 2021. http://dx.doi.org/10.1515/ijnsns-2020-0180.

[10] Abbes A, Ouannas A, Shawagfeh N, Khennaoui AA. Incommensurate fractional discrete neural network: Chaos and complexity. Eur Phys J Plus 2022;137. http://dx.doi.org/10.1140/epjp/s13360-022-02472-6.

[11] Abbes A, Ouannas A, Shawagfeh N. The incommensurate fractional discrete macroeconomic system: Bifurcation, chaos and complexity. Chin Phys B 2022. http://dx.doi.org/10.1088/1674-1056/ac7296.

[12] Shukla MK, Sharma BB. Investigation of chaos in fractional order generalized hyperchaotic Henon map. AEU - Int J Electr Commun 2017;78:265–73. http://dx.doi.org/10.1016/j.aeue.2017.05.009.

[13] Ouannas A, Khennaoui AA, Momani S, Grassi G, Pham V-T. Chaos and control of a three-dimensional fractional order discrete-time system with no equilibrium and its synchronization. AIP Adv 2020;10:045310. http://dx.doi.org/10.1063/5.0004884.

[14] Ouannas A, Khennaoui AA, Wang X, Pham V-T, Boulaaras S, Momani S. Bifurcation and chaos in the fractional form of Hénon-Lozi type map. Eur Phys J Spec Top 2020;229:2261–73. http://dx.doi.org/10.1140/epjst/e2020-900193-4.

[15] Gasri A, Khennaoui A-A, Ouannas A, Grassi G, Iatropoulos A, Moysis L, et al. A new fractional-order map with infinite number of equilibria and its encryption application. Complexity 2022;2022:1–18. http://dx.doi.org/10.1155/2022/3592422.

[16] Khennaoui A-A, Ouannas A, Bendoukha S, Grassi G, Lozi RP, Pham V-T. On fractional–order discrete–time systems: Chaos, stabilization and synchronization. Chaos Solitons Fractals 2019;119:150–62. http://dx.doi.org/10.1016/j.chaos.2018.12.019.

[17] Alaoui AL, Tilioua M, Ammi MRSidi, Agarwal P. Dynamical analysis of a Caputo fractional order sir epidemic model with a general treatment function. Infosys Sci Found Ser 2021;17–33. http://dx.doi.org/10.1007/978-981-16-2450-6_2.

[18] Parsamanesh M, Erfanian M. Stability and bifurcations in a discrete-time SIVS model with saturated incidence rate. Chaos Solitons Fractals 2021;150:111178. http://dx.doi.org/10.1016/j.chaos.2021.111178.

[19] Meiksin A. Using the SEIR model to constrain the role of contaminated fomites in spreading an epidemic: An application to COVID-19 in the UK. Math Biosci Eng 2022;19:3564–90. http://dx.doi.org/10.3934/mbe.2022164.

[20] He Z-Y, Abbes A, Jahanshahi H, Alotaibi ND, Wang Y. Fractional-order discrete-time sir epidemic model with vaccination: Chaos and complexity. Mathematics 2022;10:165. http://dx.doi.org/10.3390/math10020165.

[21] Anggriani N, Ndii MZ, Amelia R, Suryaningrat W, Pratama MA. A mathematical covid-19 model considering asymptomatic and symptomatic classes with waning immunity. Alex Eng J 2022;61:113–24. http://dx.doi.org/10.1016/j.aej.2021.04.104.

[22] Zhang Z, Zeb A, Egbelowo OF, Erturk VS. Dynamics of a fractional order mathematical model for covid-19 epidemic. Adv Difference Equ 2020;2020:1–16. http://dx.doi.org/10.1186/s13662-020-02873-w.
[23] Ogunrinde RB, Nwajeri UK, Fadugba SE, Ogunrinde RR, Oshinubi KI. Dynamic model of COVID-19 and citizens reaction using fractional derivative. Alex Eng J 2021;60:2001–12. http://dx.doi.org/10.1016/j.aej.2020.09.016.
[24] Majee S, Adak S, Jana S, Mandal M, Kar TK. Complex dynamics of a fractional-order sir system in the context of covid-19. J Appl Math Comput 2022;1–24. http://dx.doi.org/10.1007/s12190-021-01681-z.
[25] Akindeinde SO, Okyere E, Adewumi AO, Lebelo RS, Fabelurin OO, Moore SE. Caputo fractional-order SEIRP model for covid-19 pandemic. Alex Eng J 2022;61:829–45. http://dx.doi.org/10.1016/j.aej.2021.04.097.
[26] Nisar KS, Ahmad S, Ullah A, Shah K, Alrabaiah H, Arfan M. Mathematical analysis of SIRD model of COVID-19 with Caputo fractional derivative based on real data. Results Phys 2021;21:103772. http://dx.doi.org/10.1016/j.rinp.2020.103772.
[27] ELSONBATY AMR, SABIR ZULQURNAIN, RAMASWAMY RAJAGOPALAN, ADEL WALEED. Dynamical analysis of a novel discrete fractional SITRS model for COVID-19. Fractals 2021;29. http://dx.doi.org/10.1142/s0218348x21400351.
[28] Aldawish I, Ibrahim RW. A new mathematical model of multi-faced COVID-19 formulated by fractional derivative chains. Adv Contin Discrete Model 2022;2022. http://dx.doi.org/10.1186/s13662-022-03677-w.
[29] Kuddus MA, Rahman A. Analysis of COVID-19 using a modified SLIR model with nonlinear incidence. Results Phys 2021;27:104478. http://dx.doi.org/10.1016/j.rinp.2021.104478.
[30] Lounis M, Bagal DK. Estimation of sir model's parameters of COVID-19 in Algeria. Bull Natl Res Centre 2020;44. http://dx.doi.org/10.1186/s42269-020-00434-5.
[31] Zhuang Y, Chen Y. Risk management of covid-19 epidemic spread in urban rail transit based on SEIR model. In: Sixth international conference on electromechanical control technology and transportation. 2022, http://dx.doi.org/10.1117/12.2624679.
[32] Sitthiwirattham T, Zeb A, Chasreechai S, Eskandari Z, Tilioua M, Djilali S. Analysis of a discrete mathematical COVID-19 model. Results Phys 2021;28:104668. http://dx.doi.org/10.1016/j.rinp.2021.104668.
[33] Abdeljawad T. On Riemann and Caputo fractional differences. Comput Math Appl 2011;62:1602–11. http://dx.doi.org/10.1016/j.camwa.2011.03.036.
[34] Atici FM, Eloe P. Discrete fractional calculus with the Nabla operator. Electron J Qual Theory Differ Equ 2009;1–12. http://dx.doi.org/10.14232/ejqtde.2009.4.3.
[35] van den Driessche P, Watmough J. Reproduction numbers and sub-threshold endemic equilibria for compartmental models of disease transmission. Math Biosci 2002;180:29–48. http://dx.doi.org/10.1016/s0025-5564(02)00108-6.
[36] Čermák J, Györi I, Nechvátal L. On explicit stability conditions for a linear fractional difference system. Fract Calc Appl Anal 2015;18:651–72. http://dx.doi.org/10.1515/fca-2015-0040.
[37] Wu G-C, Baleanu D. Discrete fractional logistic map and its chaos. Nonlinear Dynam 2013;75(1):283–7. http://dx.doi.org/10.1007/s11071-013-1065-7.
[38] Wu G-C, Baleanu D. Jacobian matrix algorithm for Lyapunov exponents of the discrete fractional maps. Commun Nonlinear Sci Numer Simul 2015;22:95–100. http://dx.doi.org/10.1016/j.cnsns.2014.06.042.
[39] Ran J. Discrete chaos in a novel two-dimensional fractional chaotic map. Adv Difference Equ 2018;2018. http://dx.doi.org/10.1186/s13662-018-1760-2.
[40] COVID live - coronavirus statistics - worldometer, worldometers.info. 2022, https://www.worldometers.info/coronavirus. [Accessed 22 February 2022].
[41] Khan AQ, Tasneem M, Almatrafi MB. Discrete-time covid-19 epidemic model with bifurcation and control. Math Biosci Eng 2021;19:1944–69. http://dx.doi.org/10.3934/mbe.2022092.
[42] Population - worldometer, worldometers.info. 2022, https://www.worldometers.info/population. [Accessed 22 February 2022].
[43] Gatto M, Bertuzzo E, Mari L, Miccoli S, Carraro L, Casagrandi R, et al. Spread and dynamics of the covid-19 epidemic in Italy: Effects of emergency containment measures. Proc Natl Acad Sci 2020;117:10484–91. http://dx.doi.org/10.1073/pnas.2004978117.